

~~RESTRICTED~~

COPY NO. 162  
RM No. E9C16

NACA RM No. E9C16

E9C16



TECH LIBRARY KAFB, NM

NACA

# RESEARCH MEMORANDUM

EXPERIMENTAL INVESTIGATION OF HOT-GAS BLEEDBACK  
FOR ICE PROTECTION OF TURBOJET ENGINES  
II - NACELLE WITH LONG STRAIGHT AIR INLET

By Edmund E. Callaghan and Robert S. Ruggeri

Lewis Flight Propulsion Laboratory  
Cleveland, Ohio

CLASSIFIED DOCUMENT

This document contains classified information affecting the National Defense of the United States within the meaning of the Espionage Act, USC 50:31 and 32. No transmission or the revelation of its contents in any manner to an unauthorized person is prohibited by law. Information so classified may be imparted only to persons in the military and naval services of the United States, appropriate civilian officers and employees of the Federal Government who have a legitimate interest therein, and to United States citizens of known loyalty and discretion who of necessity must be informed thereof.

AFM-6  
TECHNICAL LIBRARY  
APL 2811

## NATIONAL ADVISORY COMMITTEE FOR AERONAUTICS

WASHINGTON  
May 26, 1949

~~RESTRICTED~~

6583

*Declassified by Authority of LARC Security Classification  
Officer (SC) Letter, Dated June 16, 1983*

*Martin Sommer*

*519.98/13*

Langley Research Center  
Hampton, Virginia  
23665

100

Reply to Attn of

139A

JUN 16 1983

TO: Distribution

FROM: 180A/Security Classification Officer

SUBJECT: Authority to Declassify NACA/NASA Documents Dated Prior to  
January 1, 1960

*(informal correspondence)*  
Effective this date, all material classified by this Center prior to  
January 1, 1960, is declassified. This action does not include material  
derivatively classified at the Center upon instructions from other Agencies.

Immediate re-marking is not required; however, until material is re-marked by  
lining through the classification and annotating with the following statement,  
it must continue to be protected as if classified:

"Declassified by authority of LARC Security Classification Officer (SCO)  
letter dated June 16, 1983," and the signature of person performing the  
re-marking.

If re-marking a large amount of material is desirable, but unduly burdensome,  
custodians may follow the instructions contained in NHB 1640.4, subpart F,  
section 1203.604, paragraph (h).

This declassification action complements earlier actions by the National  
Archives and Records Service (NARS) and by the NASA Security Classification  
Officer (SCO). In Declassification Review Program 807008, NARS declassified  
the Center's "Research Authorization" files, which contain reports, Research  
Authorizations, correspondence, photographs, and other documentation.  
Earlier, in a 1971 letter, the NASA SCO declassified all NACA/NASA formal  
series documents with the exception of the following reports, which must  
remain classified:

Document No.

First Author

E-51A30  
E-53G20  
E-53G21  
E-53K18  
SL-54J21a  
E-55C16  
E-56H23a

Nagey  
Francisco  
Johnson  
Spooner  
Westphal  
Fox  
Himmel

JUN 23 1983

if you have any questions concerning this matter, please call Mr. William L. Simkins at extension 3281.

  
Jess G. Ross  
2898

Distributions:  
SDL 031

cc:

NASA Scientific and Technical  
Information Facility  
P.O. Box 8757  
BWI Airport, MD 21240

NASA--NIS-5/Security  
180A/RIAD  
139A/TU&AO

*6-15-83*  
139A/WLSimkins:elf 06/15/83 (3281)

139A/JS *6-15-83*

BLOC 1194

MAIL STOP 188

HEADS OF ORGANIZATIONS  
JANE S. HESS



## NATIONAL ADVISORY COMMITTEE FOR AERONAUTICS

RESEARCH MEMORANDUM

## EXPERIMENTAL INVESTIGATION OF HOT-GAS BLEEDBACK

## FOR ICE PROTECTION OF TURBOJET ENGINES

## II - NACELLE WITH LONG STRAIGHT AIR INLET

By Edmund E. Callaghan and Robert S. Ruggeri

## SUMMARY

Aerodynamic and icing investigations were conducted in the NACA Lewis icing research tunnel on a two-thirds-scale model of a turbojet-engine nacelle with a long straight air inlet in order to provide basic design criterions for hot-gas bleedback systems. An investigation of a hot-gas bleedback system consisting of several orifices peripherally located around the inlet opening was conducted for both dry-air and icing conditions. General rules for obtaining a satisfactory orifice configuration are presented.

The most uniform temperature distribution was obtained with a bleedback of 4.4 percent at a gas temperature of  $1000^{\circ}$  F and resulted in an average dry-air-temperature rise of  $46^{\circ}$  F. The maximum deviation from the average air-temperature rise for this condition was  $6^{\circ}$  F. Satisfactory agreement between calculated and measured heat requirements for icing conditions was obtained.

## INTRODUCTION

As part of a general program to provide icing protection for turbojet engines, a nacelle with several air inlets is being experimentally investigated at the NACA Lewis laboratory to establish a reasonable design criterion for hot-gas bleedback systems.

The investigation described herein is a continuation of the general program outlined in reference 1 and was conducted with the same turbojet-engine nacelle, but with a long straight air inlet. The nacelle was two-thirds full scale. The model was provided with orifices for introducing hot gas into the inlet. Data were obtained to determine the effect of gas temperature and pressure, tunnel velocity, and angle of attack on the temperature distribution at the

simulated engine inlet. In addition, data were obtained to validate the use of the jet-penetration equation (reference 2) as applied to a three-dimensional duct. The icing investigation to determine the minimum heat requirements was conducted over a range of liquid-water contents from 0.3 to 1.0 gram per cubic meter and at a free-stream total temperature of 0° F with the model at angles of attack of 0° and 8°.

A design procedure for obtaining a satisfactory orifice configuration is presented in the appendix.

### APPARATUS

The nacelle investigated was similar to the offset-air-inlet nacelle described in reference 1, but had a long, circular, and straight air inlet. The model as installed in the tunnel test section is shown in figure 1. The model was two-thirds full scale and was constructed of steel, Inconel, and aluminum. The inlet length from the nacelle lip to the accessory housing was 53 inches. The inlet area at stagnation was 1.227 square feet and the area at the inlet minimum section was 0.835 square foot. The orifices through which the hot gas was discharged were located at the minimum section 5.75 inches from the nacelle lip. The hot gas was obtained by passing high-pressure air through a combustion heater and ducting the air to the model. The model was designed for a maximum air flow of 32 pounds per second, corresponding to the flow through a full-scale axial-flow engine of 4000 pounds static thrust at sea level with an 11-stage compressor, eight cylindrical burners, and a single-stage turbine. A 1/4-inch mesh, 0.050-inch-diameter wire screen was mounted in the model (fig. 2) to simulate a protective screen installation and to provide a means of indicating icing.

### INSTRUMENTATION

The model instrumentation used in the investigation is shown in figure 2. Measurements were made of mass flow, ram-pressure recovery, temperature distribution at the simulated engine inlet, pressure drop across the screen, and air temperature ahead of and behind the screen. The model aft of the temperature cross rake (fig. 2) is the same as that used in the offset-inlet investigation (reference 1). A detailed description of the instrumentation is presented in reference 1.

The inlet duct of the model was instrumented with three thermocouple rakes located 13.2, 23.1, and 33.1 inches downstream of a plane

through the orifice center lines. In each case the probes were spaced 1/2 inch apart with the outer probe coinciding with the model center line. The rakes were located directly behind a 3/4-inch-diameter orifice. The average air temperature and temperature distribution inside the model were measured by means of a thermocouple cross rake mounted in the duct 43 inches downstream of the orifices and just ahead of the simulated accessory housing, as shown in figure 2. The rake consisted of 29 total-temperature thermocouples spaced 1 inch apart and mounted in two streamlined struts intersecting at 90°. Temperatures on the surface of the inlet duct were measured by 47 flush-type thermocouples, 30 of which were mounted in the duct wall and 17 on the accessory housing.

The state of the gas in the plenum chamber was measured by four thermocouple probes located 90° apart in the plane of the orifices and by four static-pressure taps in the rear wall of the plenum chamber.

The nacelle-lip pressure distribution was measured by means of pressure belting cemented to the lip surface. Lip-temperature distribution was measured by thermocouples welded to the nacelle lip.

Air flow through the model and inlet-velocity ratio were controlled by an electrically driven tail cone (fig. 2).

#### SYMBOLS

The following symbols are used in this report:

$A_i$	inlet area at orifices, square feet
$A_j$	total area of orifices (jet area), square feet
$A_s$	free area through screen, 0.732 square foot
$c_p$	specific heat of air, Btu per pound °F
$c_{p,g}$	specific heat of gas, Btu per pound °F
$c_{p,w}$	specific heat of water, Btu per pound °F
$D_j$	diameter of orifice (jet diameter), inches
$g$	acceleration due to gravity, 32.2 feet per second per second
$J$	mechanical equivalent of heat, 778 foot-pounds per Btu

L	latent heat of vaporization of water, Btu per pound
l	depth of jet penetration into air stream at distance s downstream of orifice center line, inches
m	liquid-water content, pounds water per pound air
$P_f$	total pressure at front rakes, pounds per square foot absolute
$P_j$	jet total pressure, inches of mercury absolute
$P_0$	free-stream total pressure, pounds per square foot absolute
p	local surface static pressure, pounds per square foot absolute
$P_0$	free-stream static pressure, pounds per square foot absolute
$\Delta p$	static-pressure drop across screen, pounds per square foot
q	dynamic pressure ahead of screen, pounds per square foot
$q_0$	free-stream dynamic pressure, pounds per square foot
S	pressure coefficient, $1 - \left( \frac{p - P_0}{q_0} \right)$
s	distance downstream of orifice center line or mixing distance, inches
$T_{av}$	model-air total temperature (area weighted), °F
$T_g$	plenum-chamber gas temperature, °F
$T_j$	total temperature of jet ( $T_g + 460$ ), °R
$T_x$	local air total temperature in model, °F
$T_0$	free-stream total temperature, °F
$V_1$	inlet-stream velocity at orifices, feet per second
$V_j$	velocity of jet at vena contracta, feet per second
$V_s$	velocity through screen, feet per second

$W_a$	mass flow through model, pounds per second
$W_d$	design mass flow through model, pounds per second
$W_g$	hot-gas flow through orifices, pounds per second
$W_B$	saturated vapor content, pounds water per pound dry air
$\beta$	bleedback ( $W_g/W_a \times 100$ ), percent
$\eta$	ram-pressure recovery, $1 - \left( \frac{P_0 - P_f}{q_0} \right)$
$\eta_{calc}$	calculated ram-pressure recovery
$\rho_a$	density of air in model, slugs per cubic foot
$\rho_d$	design free-stream density, slugs per cubic foot
$\rho_i$	mass density of inlet stream at orifices, slugs per cubic foot
$\rho_j$	mass density of jet at vena contracta, slugs per cubic foot
$\rho_0$	mass density of free stream, slugs per cubic foot

#### PROCEDURE

Aerodynamic investigation without bleedback. - An aerodynamic investigation of the model without orifices was conducted to determine air-flow characteristics, lip-pressure distribution, and ram-pressure recovery as a function of inlet-velocity ratio and angle of attack. The range of tunnel-air velocities was from approximately 200 to 400 feet per second. At each tunnel velocity investigated, the angle of attack was varied from  $0^\circ$  to  $8^\circ$  and for each angle of attack the inlet-velocity ratio was varied from 0.64 to 0.82.

Aerodynamic investigation with cold-gas bleedback. - An aerodynamic investigation of the model with orifices was conducted to determine the effect of cold-gas bleedback on air-flow characteristics, lip-pressure distribution, and ram-pressure recovery. This investigation was conducted at an angle of attack of  $0^\circ$  at a fixed tail-cone position corresponding to an inlet-velocity ratio of 0.82 without bleedback. The tunnel-air velocities ranged from 200 to 460 feet per second and bleedback ranged from 2.4 to 10.4 percent.

Aerodynamic investigation with hot-gas bleedback. - Several orifice configurations were investigated in order to obtain a configuration that would give a uniform temperature distribution inside the model for a range of values of tunnel velocity, angle of attack, gas flow, and gas temperature. The configuration selected is shown in figure 3 and consists of three  $\frac{3}{4}$ -inch, three  $\frac{1}{2}$ -inch, and six  $\frac{13}{32}$ -inch orifices. Calculated jet outlines and penetrations are also shown in figure 3 and the method by which these outlines and penetrations were obtained is discussed in the appendix.

The effect of hot-gas bleedback on the temperature distribution inside the model, on the air-flow characteristics, and on the ram-pressure recovery for the optimum orifice configuration was determined as a function of tunnel velocity, angle of attack, gas flow, and gas temperature. The investigation was conducted at a fixed tail-cone position corresponding to an inlet-velocity ratio of 0.82 without bleedback and at a free-stream total temperature of 0° F for tunnel velocities from 200 to 470 feet per second and angles of attack from 0° to 8°. Gas flows and plenum-chamber gas temperatures ranged from 0.52 to 1.73 pounds per second and from approximately 600° to 1000° F, respectively. For each plenum-chamber gas temperature, the gas pressure was varied from 2900 to 6000 pounds per square foot absolute.

Icing with hot-gas bleedback. - An investigation to determine the critical-icing criterion as a function of mass air flow, gas flow, angle of attack, and liquid-water content for a constant free-stream total temperature of 0° F was conducted in the same manner as that of reference 1. This investigation was conducted at tunnel velocities of 200, 280, 360, and 410 feet per second at angles of attack of 0° and 8°. The liquid-water content ranged from 0.3 to 1.0 gram per cubic meter at an average drop diameter of 15 microns. The range of gas flows and plenum-chamber gas temperatures was the same as that employed for the aerodynamic investigation with hot-gas bleedback.

## RESULTS AND DISCUSSION

### Aerodynamic Investigation without Bleedback

Mass-flow characteristics. - The mass flow through the model increased nearly linearly with tunnel velocity for a fixed tail-cone position and angle of attack. A maximum flow of approximately 31.4 pounds per second was obtained at an inlet-velocity ratio of 0.82, a tunnel velocity of 470 feet per second, and an angle of attack of 0°.

Ram-pressure recovery. - A ram-pressure recovery  $\eta$  of approximately 0.95 was obtained at an angle of attack of  $0^\circ$  and an inlet-velocity ratio of 0.82. No appreciable change in ram-pressure recovery was observed for an increase in angle of attack from  $0^\circ$  to  $8^\circ$  and a decrease in inlet-velocity ratio from 0.82 to 0.64.

Lip-pressure distribution. - The effect of angle of attack on lip-pressure distribution is shown in figure 4. The pressure distribution is presented in terms of a pressure coefficient

$$S = 1 - \left( \frac{p - p_0}{q_0} \right)$$

#### Aerodynamic Investigation with Cold-Gas Bleedback

Mass-flow characteristics. - No measurable decrease in mass flow through the model was observed with increasing bleedback. A decreasing inlet-velocity ratio must therefore occur with increasing bleedback because an increasing part of the total flow through the model is represented by the bleedback gas and as a consequence the flow entering the inlet is reduced.

Ram-pressure recovery. - In order to determine the effect of the jets alone, cold gas was bled into the inlet air stream; the effect of bleedback on ram-pressure recovery  $\eta$  is shown in figure 5 for a free-stream total temperature of  $0^\circ$  F and tunnel velocities of 220, 300, 380, and 450 feet per second. Figure 5 shows that the loss in ram-pressure recovery is linearly related to bleedback and no effect of velocity on ram-pressure recovery is evident.

Lip-pressure distribution. - A slight movement of the stagnation point to a position farther inside the lip was observed with cold-gas bleedback. This movement increased with increasing bleedback (fig. 6) and was caused by the decrease in the inlet-velocity ratio with increasing bleedback. The decreased inlet velocity was further evidenced by the reduced pressure coefficients in the inlet.

#### Aerodynamic Investigation with Hot-Gas Bleedback

Optimum orifice configuration. - Several orifice configurations were investigated in order to obtain an optimum configuration that would give the most uniform temperature distribution at the simulated engine inlet. Results are presented for the orifice configuration that gave the most uniform temperature distribution at the calculated value of bleedback (4.4 percent) and gas temperature ( $1000^\circ$  F) necessary for adequate ice prevention corresponding to an icing condition

with a free-stream total temperature of  $0^{\circ}$  F and a liquid-water content of 1.0 gram per cubic meter. A procedure for obtaining a satisfactory orifice configuration is presented in the appendix.

Model-air temperature distribution. - When the penetration equation of reference 2

$$\left(\frac{l}{D_j}\right)^{1.65} = 2.91 \frac{\rho_j V_j}{\rho_1 V_1} \sqrt{\frac{S}{D_j}}$$

is utilized, it is apparent that the penetration is a function of the product of the density and the velocity ratios because the geometric parameters are fixed. The total jet area  $A_j$  and the inlet area

$A_1$  of the model are fixed; hence the penetration becomes a function of the bleedback because

$$l = f \left( \frac{\rho_j V_j A_j}{\rho_1 V_1 A_1} \right) = f \left( \frac{W_j}{W_a} \right)$$

After a single value of bleedback (4.4 percent) corresponding to the most uniform temperature distribution is determined, it should be possible to maintain this optimum temperature distribution for a range of tunnel velocities if the bleedback is held constant. Because the air flow through the model varies nearly linearly with tunnel velocity, the variation of gas flow must also be nearly linear in order to maintain constant bleedback. For a fixed gas temperature, the gas flow varies linearly with gas pressure for a choked jet and nearly linearly with gas pressure for a high subsonic jet. The gas pressure and the tunnel velocity should therefore be linearly related for a fixed temperature distribution. The plenum-chamber gas pressure corresponding with optimum temperature distribution was determined for a value of gas temperature of  $1000^{\circ}$  F as a function of tunnel velocity, and the variation of gas pressure with tunnel velocity was found to be linear (fig. 7). For each tunnel velocity, the experimental value of bleedback proved to be the same (4.4 percent) and resulted in identical average air-temperature rises of  $46^{\circ}$  F with a maximum deviation of  $6^{\circ}$  F.

The effect of employing gas pressures other than the optimum (3950 lb/sq ft) is illustrated in figure 8 for a tunnel velocity of 290 feet per second and a plenum-chamber gas temperature of  $1000^{\circ}$  F. Lines of constant total-temperature ratio  $T_x/T_{av}$  are

indicated for plenum-chamber gas pressures of 3010, 3950, 5100, and 5840 pounds per square foot absolute. The use of a pressure lower than the optimum results in low temperature ratios at the center with increasing temperature ratios near the duct walls (fig. 8(a)). For the plenum-chamber gas pressures higher than the optimum, the region of highest temperature ratio occurred at the center of the model and decreasing temperature ratios were encountered as the distance from the center increased (figs. 8(c) and 8(d)). A comparison of figures 8(a) to 8(d) shows that increasing temperature ratios are obtained near the center of the model with increasing gas pressures. In addition, the temperature-ratio gradient becomes more severe with increasing pressure.

The effect of angle of attack on the temperature distribution was negligible and almost no change in distribution was obtained when the other factors were maintained constant.

Increasing the plenum-chamber gas temperature at a fixed angle of attack also had very little effect on the temperature distribution aside from increasing the temperature rise; nearly identical total-temperature-ratio contours were obtained at constant tunnel speed and plenum-chamber gas pressure.

Mass-flow loss. - A reduction in mass flow through the model occurred with increasing model-air total temperature at a fixed tunnel velocity, free-stream total temperature, and angle of attack. The decrease in mass flow with increasing model-air temperature for several values of tunnel velocity and an angle of attack of  $0^\circ$  is shown in figure 9. The decrease in mass flow is linearly related to the model-air temperature for a fixed tunnel velocity. The reduction in flow is due to the decrease in air density associated with increasing temperature, which indicates that the effect of compressibility and the changes in static pressure inside the model with bleedback have a negligible effect on mass flow. At a fixed tunnel velocity, the model therefore operates as a constant-volume machine.

Ram-pressure recovery. - The ram-pressure loss associated with the addition of heat by jets directed perpendicularly to a moving air stream consists of two components. The first component arises from the momentum pressure loss associated with changing the direction of the jets. The other component arises from the change in density of the air due to the addition of heat. The effect of the first component is illustrated in figure 5. Because the model is a constant-volume machine and the velocities through the model are sufficiently low that compressibility effects may be neglected, the ram-pressure loss due to

heat addition can be written as  $q_0 \left( 1 - \frac{460 + T_0}{460 + T_{av}} \right)$ . The  $\eta_{calc}$  curve of figure 10 was calculated from the data of figure 5, assuming a tunnel total temperature of  $0^\circ$  F, a plenum-chamber gas temperature of  $1000^\circ$  F, and perfect mixing. The lower curve in figure 10 was computed by subtracting the quantity  $\left( 1 - \frac{460 + T_0}{460 + T_{av}} \right)$  from the upper curve. The experimental data also plotted in figure 10 for a gas temperature of  $1000^\circ$  F show good agreement with the computed curve.

Inlet-lip temperature distribution. - The maximum inlet-lip temperatures were obtained at the highest value of bleedback and plenum-chamber gas temperature utilized in the investigation. The maximum lip temperatures encountered are shown in figure 11 and were obtained at a bleedback of 8.65 percent and a plenum-chamber gas temperature of  $1000^\circ$  F. The lip temperatures decreased with decreasing bleedback or decreasing plenum-chamber gas temperature.

Duct-skin temperature. - The highest measured duct-skin temperature was  $185^\circ$  F and was obtained at a point on the skin adjacent to the hot-gas ducts, which were located in the inlet wall. The model-air total temperature was approximately  $90^\circ$  F and the plenum-chamber gas temperature,  $1000^\circ$  F. For an average air-temperature rise of  $40^\circ$  F, the skin temperature did not exceed  $100^\circ$  F. The temperature of the skin, except adjacent to the hot-gas ducting, did not exceed the model-air total temperature.

#### Icing with Bleedback

In the analysis of the icing data, the pressure-drop coefficients  $\Delta p/q$  across the screen were computed for each icing run. The screen was considered iced when the value of  $\Delta p/q$  approached 1.5 times the value for the screen at the beginning of each run. The experimental bleedback and plenum-chamber gas temperatures corresponding to this criterion are shown in figure 12 for tunnel velocities of 200, 280, 360, and 410 feet per second at an angle of attack of  $0^\circ$  and for 200 and 280 feet per second at an angle of attack of  $8^\circ$ . No ice accretions were observed on the accessory housing nor the nacelle lip when the inlet screen was iced. A very slight ice formation encountered from 4 to 10 inches behind the orifices around the entire periphery of the inlet was apparently caused by the poor mixing obtained immediately behind the orifices.

1105

The theoretical curves A and B shown in figure 12 are based on the assumption that icing occurs when the minimum kinetic temperature (static temperature plus 0.85 times the dynamic temperature) on the screen was 32° F. These curves represent the upper and lower limits of the icing conditions used in the investigation; that is, curve A was calculated for saturated air at 0° F, a tunnel velocity of 410 feet per second, and a liquid-water content of 1.0 gram per cubic meter. Curve B was calculated for saturated air at 0° F, a tunnel velocity of 220 feet per second, and a liquid-water content of 0.7 gram per cubic meter.

In order to assure a minimum kinetic temperature of 32° F on the screen, an average kinetic temperature of 38° F and a total temperature of 41.3° F are required at a tunnel velocity of 410 feet per second, corresponding to a velocity in the screen of 516 feet per second; a total temperature of 39.4° F is required at a tunnel velocity of 220 feet per second, corresponding to a velocity in the screen of 302 feet per second.

Nearly all the data in figure 12 fall within the limits of the two curves. If the conditions of the investigation had been ideal, the lower-speed data would have fallen near curve B and the higher-speed data near curve A, provided that the liquid-water content in all cases was constant. The variation in liquid-water content and the use of other than the optimum amount of bleedback preclude such a correlation.

Inlet-lip temperature distribution. - A marked reduction in inlet-lip temperature, particularly near the stagnation region, was observed under icing conditions as compared with nonicing conditions. Typical lip-temperature profiles for both conditions are shown in figure 13 for a bleedback of 4.4 percent and a plenum-chamber gas temperature of 1000° F. The liquid-water content for the icing condition was 0.5 gram per cubic meter.

#### SUMMARY OF RESULTS

The following results were obtained from an icing-research-tunnel investigation of a two-thirds-scale model of a turbojet-engine nacelle with a long straight air inlet utilizing a hot-gas bleedback system for ice prevention:

1. Identical temperature distributions were obtained at the simulated engine inlet for a fixed amount of bleedback independent of tunnel velocity.

2. Optimum temperature distribution was obtained at a bleedback of 4.4 percent. This value of bleedback resulted in an average dry-air-temperature rise of 46° F with a maximum local temperature deviation of 6° F at the engine inlet for a gas temperature of 1000° F.

3. The use of plenum-chamber gas pressure other than the optimum resulted in increased temperature gradients across the inlet. For pressures higher than the optimum, low-temperature regions existed near the duct walls and for pressures lower than optimum the low-temperature regions occurred at the duct center.

4. The introduction of cold gas under pressure through the orifices decreased the ram-pressure recovery linearly with increasing bleedback. The ram-pressure recovery with hot-gas bleedback decreased nearly linearly with increasing average model-air temperature.

5. The decrease in mass flow with hot-gas bleedback was almost entirely attributable to the decrease in air density resulting from the increase in air temperature in the model.

6. Satisfactory agreement was obtained between the calculated heat requirements and the measured heat requirements for icing conditions.

#### CONCLUDING REMARKS

The foregoing discussion indicates that it is possible by means of analysis to obtain a satisfactory orifice configuration for the protection of a jet-engine nacelle by hot-gas bleedback and to predict many of its thermodynamic and aerodynamic characteristics. The change in mass flow and the reduction in ram-pressure recovery due to the addition of heat can be accurately computed. It has been established that the temperature distribution at the engine inlet is a function of bleedback alone and that the amount of bleedback required for a given icing condition can be accurately calculated.

Lewis Flight Propulsion Laboratory,  
National Advisory Committee for Aeronautics,  
Cleveland, Ohio.

## APPENDIX - DESIGN PROCEDURE FOR OBTAINING TRIAL

## ORIFICE CONFIGURATION

The design procedure for obtaining a trial orifice configuration is illustrated by the following example:

Determination of bleedback necessary to maintain minimum kinetic temperature of 32° F on screen or inlet guide vanes. - The first step is to estimate the total-temperature rise needed, corresponding with the design conditions, and to determine the mass-flow reduction due to the decrease in density associated with heating the inlet air. Because the investigation was conducted at a tunnel total temperature of 0° F, the required temperature rise was estimated to be 40° F from the results of reference 1. In addition, reference 1 indicates that the mass-flow decrease is directly proportional to the decrease in density. The model investigated was designed for a mass flow of 32 pounds per second at a free-stream density of 0.0024 slug per cubic foot and a free-stream velocity of 490 feet per second. The actual air flow is therefore

$$\rho_a = \rho_d \frac{460}{460 + T_{av}} = 0.0024 \times \frac{460}{500} = 0.00221 \text{ slug/cu ft}$$

$$W_a = W_d \frac{460}{460 + T_{av}} = \frac{460}{500} \times 32.0 = 29.5 \text{ lb/sec}$$

The second step is to calculate the velocity through the screen corresponding with the corrected air flow and to determine the dynamic temperature loss in the boundary layer associated with this velocity. As a first approximation, the air density in the screen is equal to the air density in the model  $\rho_a$ . Therefore,

$$\frac{W_a}{32.2} = \rho_a V_S A_S$$

$$V_S = \frac{W_a}{32.2 \rho_a A_S} = \frac{29.5}{32.2 \times 0.00221 \times 0.732} = 568 \text{ ft/sec}$$

The dynamic temperature loss  $\Delta t$  is

$$\Delta t = \frac{0.15 V_s^2}{2 J g c_p} = \frac{(568)^2 \times 0.15}{2 \times 778 \times 32.2 \times 0.24} = 4.04^\circ \text{ F}$$

From the results of reference 1, a deviation in temperature of  $8^\circ \text{ F}$  was obtained at an average air-temperature rise of  $40^\circ \text{ F}$ . A slightly better air-temperature distribution may be expected with this model because of its symmetrical shape and a deviation of  $6^\circ \text{ F}$  was estimated. An average air-temperature rise of  $32^\circ + 4^\circ + 6^\circ \text{ F} = 42^\circ \text{ F}$  was therefore determined and the heat requirements were calculated based on a free-stream total temperature of  $0^\circ \text{ F}$ , a liquid-water content of 1.0 gram per cubic meter  $\left( 81.8 \times 10^{-5} \frac{\text{lb water}}{\text{lb air}} \right)$ , and saturated air. Because all the liquid water will be vaporized at  $10^\circ \text{ F}$  and all the vapor must be raised to the required temperature, the required heat  $H_1$  is approximately equal to

$$H_1 = c_p W_a (T_{av} - T_0) + mL (W_a - W_g) + c_{p,w} (W_a - W_g) (W_s + m) (T_{av} - T_0)$$

If a gas temperature of  $1000^\circ \text{ F}$  is assumed, the supplied heat  $H_2$  is equal to

$$H_2 = c_{p,g} W_g (T_g - T_{av})$$

Because  $H_1$  must equal  $H_2$ , however,

$$\begin{aligned} c_{p,g} W_g (T_g - T_{av}) &= c_p W_a (T_{av} - T_0) + mL (W_a - W_g) \\ &+ c_{p,w} (W_s + m) (T_{av} - T_0) (W_a - W_g) \end{aligned}$$

$$\begin{aligned} 0.26(1000-42)W_g &= 0.24 \times 29.5(42-0) + 81.8 \times 10^{-5} \times 1094(29.5-W_g) \\ &+ 1.00 (79.6 + 81.8) \times 10^{-5} (29.5-W_g)(42-0) \end{aligned}$$

$$249.9 W_g = 297.2 + 26.4 - 0.895 W_g$$

$$W_g = 1.3 \text{ lb/sec}$$

$$100 W_g / W_a = \beta = 4.4 \text{ percent}$$

When these computations were checked with a Mollier chart for saturated air, the same result was obtained.

Determination of total orifice area  $A_j$ . - The flow coefficient  $C$  of a choked jet is known to be approximately 0.87 at a plenum-chamber pressure of 80 inches of mercury and a stream static pressure of 25 inches of mercury from unpublished data. From the mass-flow equation,

$$A_j = \frac{W_g/g}{C V_j \rho_j}$$

The jet velocity and density were calculated as in reference 2, where

$$\rho_j = 0.0261 \frac{P_j}{T_j} = 0.0261 \times \frac{80}{1460} = 0.00143 \text{ slug/cu ft}$$

$$V_j = 44.8 \sqrt{T_j} = 44.8 \sqrt{1460} = 1710 \text{ ft/sec}$$

Therefore

$$A_j = \frac{1.3/32.2}{0.87 \times 0.00143 \times 1710} = 0.01890 \text{ sq ft} = 2.72 \text{ sq in.}$$

Determination of orifice configuration. - The orifice configuration was determined in accordance with the design criterions:

- (a) The total jet area must be approximately 2.72 square inches.
- (b) The layout of orifices must be symmetrical because the inlet and the ducting are symmetrical.

The area of the duct protected by a jet at a section corresponding to the position of the tip of the accessory housing was constructed for the maximum pressure and temperature available in the plenum chamber and for design free-stream velocity. The maximum available plenum-chamber temperature and pressure were 1000° F and 80 inches of mercury absolute, respectively. By use of the results of reference 2, the jet penetration for a given orifice diameter was calculated from the jet-penetration equation

$$\left(\frac{l}{D_j}\right)^{1.65} = 2.91 \frac{\rho_j V_j}{\rho_1 V_1} \sqrt{\frac{s}{D_j}}$$

where

- $l$  depth of jet penetration into air stream at distance  $s$  downstream of orifice center line measured from duct wall, in.
- $s$  distance from orifices to accessory-housing tip, 47.25 in.

The inlet-stream velocity at the orifices  $V_1$  can be determined from the mass-flow equation if it is assumed that the mass density of the inlet air was approximately equal to that of the free stream:

$$V_1 = \frac{W_a - W_g}{\rho_0 A_1 \times 32.2} = \frac{29.5 - 1.30}{32.2 \times 0.0024 \times 0.835} = 437 \text{ ft/sec}$$

The assumption of a value for the penetration  $l$  involves several considerations. First, the penetration as used in the equation of reference 2 was defined as the point at which the temperature has returned to  $1^\circ$  F above the free-stream temperature and, consequently, an allowance must be made for overlap of the jets in order that the temperatures at the simulated engine inlet be uniform. Secondly, the results of reference 2 were obtained in a straight rectangular duct, whereas the inlet ducting used in this investigation was a diffuser of  $2^\circ$  half-angle. Because the jets were introduced at the minimum area of the inlet, the jets would tend to penetrate the air stream more rapidly, not only because the wall is inclined away from the jet but also because of the decreasing air-stream velocity downstream of the jets.

The requirement for penetrations greater than those predicted by the jet-penetration equation will be partly compensated for by the effect of the diverging duct. Hence, the depth of penetration was assumed equal to that calculated from the equation of reference 2.

In order to validate this procedure for calculating penetration, the temperature profiles obtained from the three thermocouple rakes mounted in the duct were plotted and the data were analyzed in the manner of reference 2. Typical temperature profiles at the three rakes are shown in figure 14 for a tunnel velocity of 374 feet per second, a plenum-chamber gas temperature of  $837^\circ$  F, and a plenum-chamber gas pressure of 2900 pounds per square foot absolute.

It has been noted that the results of reference 2 were obtained in a rectangular duct and the penetrations were measured from a horizontal plane, whereas the profile data of figure 14 were obtained in a circular diffuser of  $2^\circ$  half-angle. The penetrations obtained from the profiles of figure 14 were based on the distance measured from the duct wall. The corresponding penetration coefficients along with the predicted values are shown in figure 15 as a function of the mixing-distance - diameter ratio. The experimental values at the simulated engine inlet are about 9 percent higher than those calculated. This increase is caused by the diverging duct.

In laying out the jet coverage, the assumption was made that the jet divergence angle was approximately  $22^\circ$ . A series of similar coverages for various sized orifices was used to facilitate laying out various orifice configurations.

1105  
Numerous orifice configurations were laid out in accordance with the design criterions. The configuration selected for trial provided the best over-all coverage with a minimum of jet overlap and represented a compromise between the two design conditions. The configuration chosen and the area protected by each jet are shown in figure 3 and the excellent results obtained with this configuration have been discussed in the text.

In order to check the design criterions and to be certain that the chosen configuration was the best, several other orifice configurations were experimentally investigated. A configuration consisting of six 3/4-inch-diameter jets equally spaced was investigated. Because of the small number of holes, very poor mixing was obtained. The screen and the accessory housing could be protected only at excessive values of bleedback. Another configuration consisting of nine holes with three 3/4-inch-diameter holes spaced at 120° intervals and two 33/64-inch-diameter holes equally spaced between the larger holes was also investigated. As in the previous configuration, poor mixing was obtained. For both of these experimental configurations, the jet layouts also showed that poor coverage would be obtained.

#### REFERENCES

1. Callaghan, Edmund E., Ruggeri, Robert S., and Krebs, Richard P.: Experimental Investigation of Hot-Gas Bleedback for Ice Protection of Turbojet Engines. I- Nacelle with Offset Air Inlet. NACA RM No. E8D13, 1948.
2. Callaghan, Edmund E., and Ruggeri, Robert S.: Investigation of the Penetration of an Air Jet Directed Perpendicularly to an Air Stream. NACA TN No. 1615, 1948.



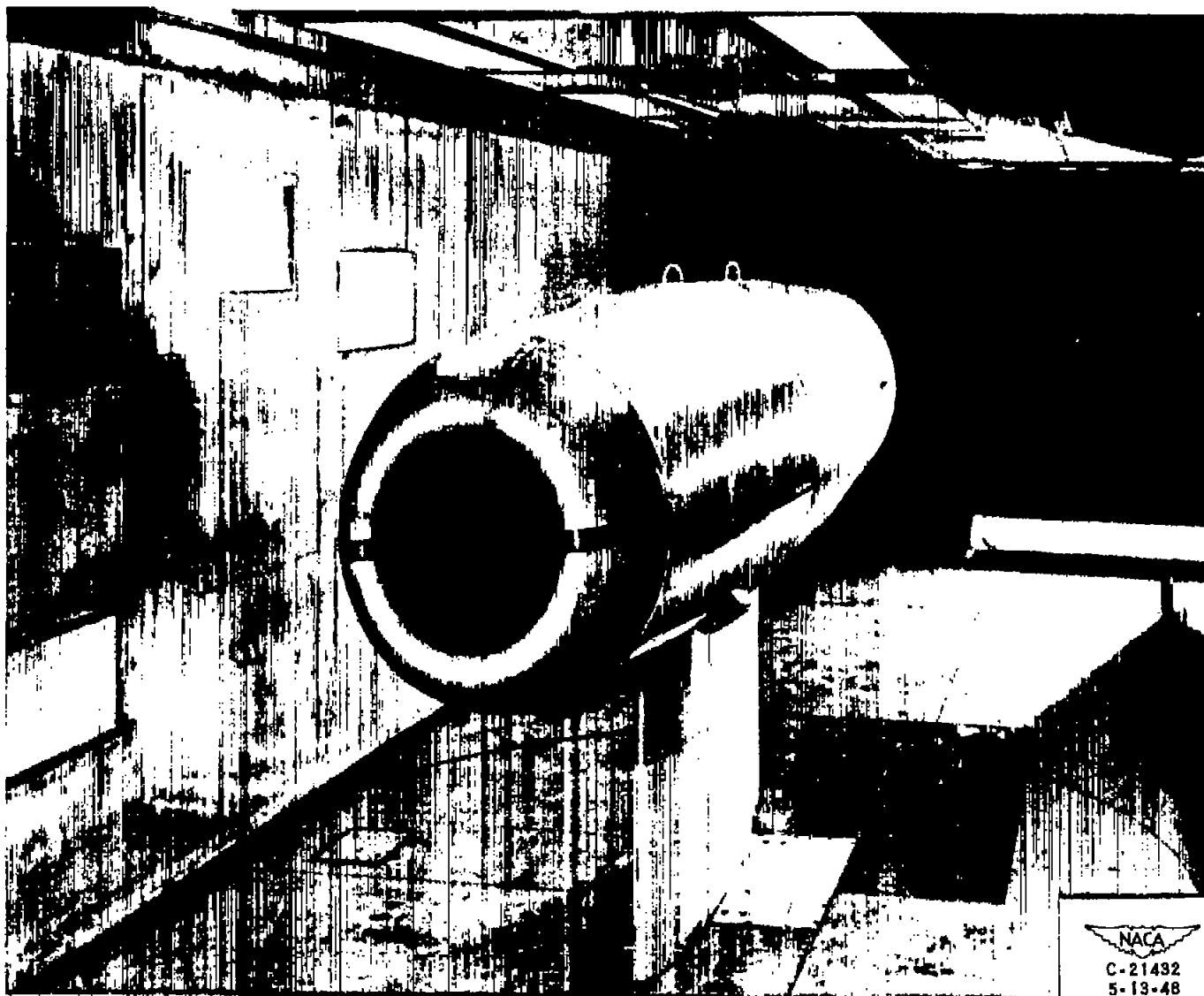
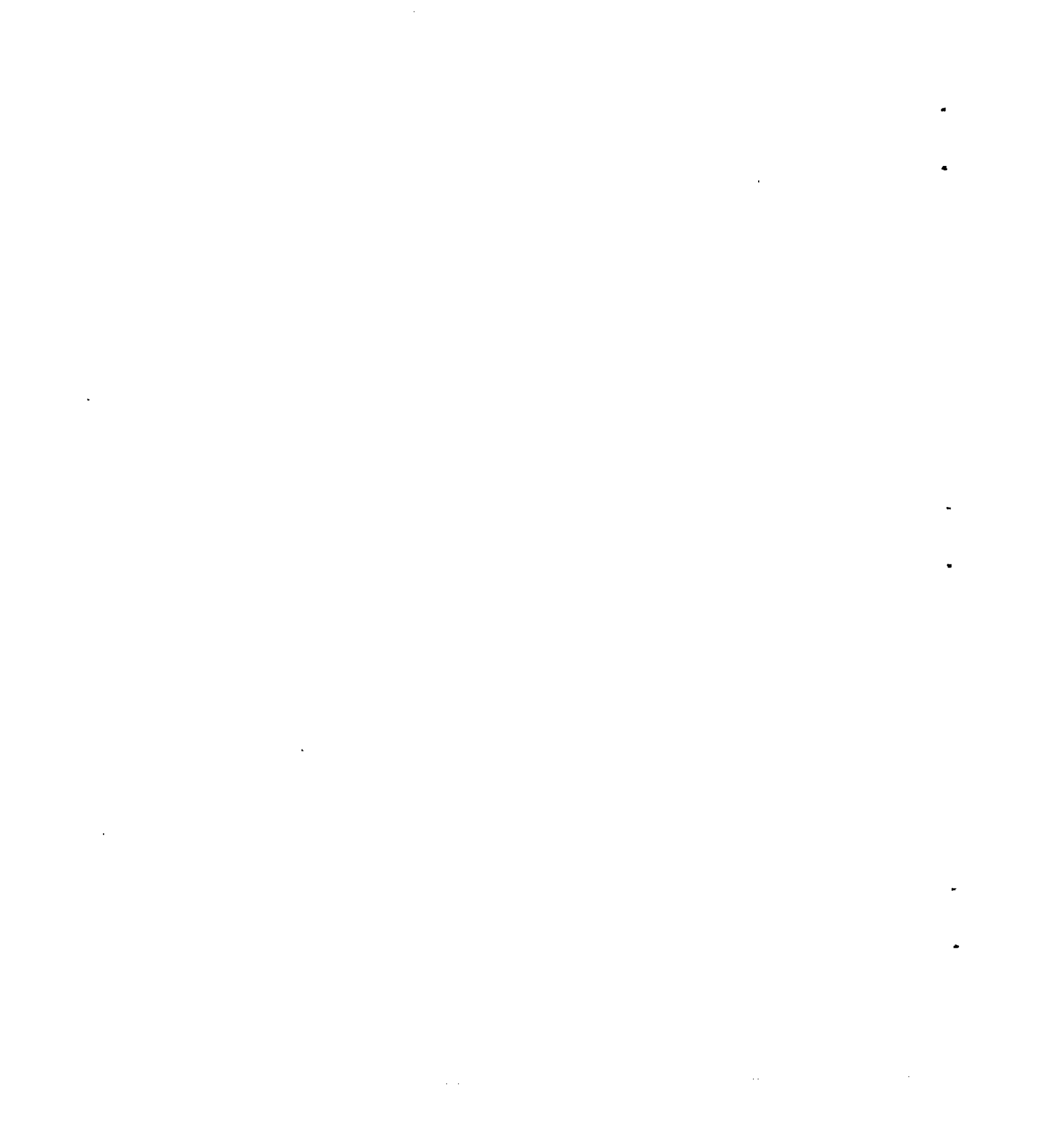


Figure 1. - Photograph of model installation in test section of icing research tunnel.

NACA  
C-21432  
5-13-48



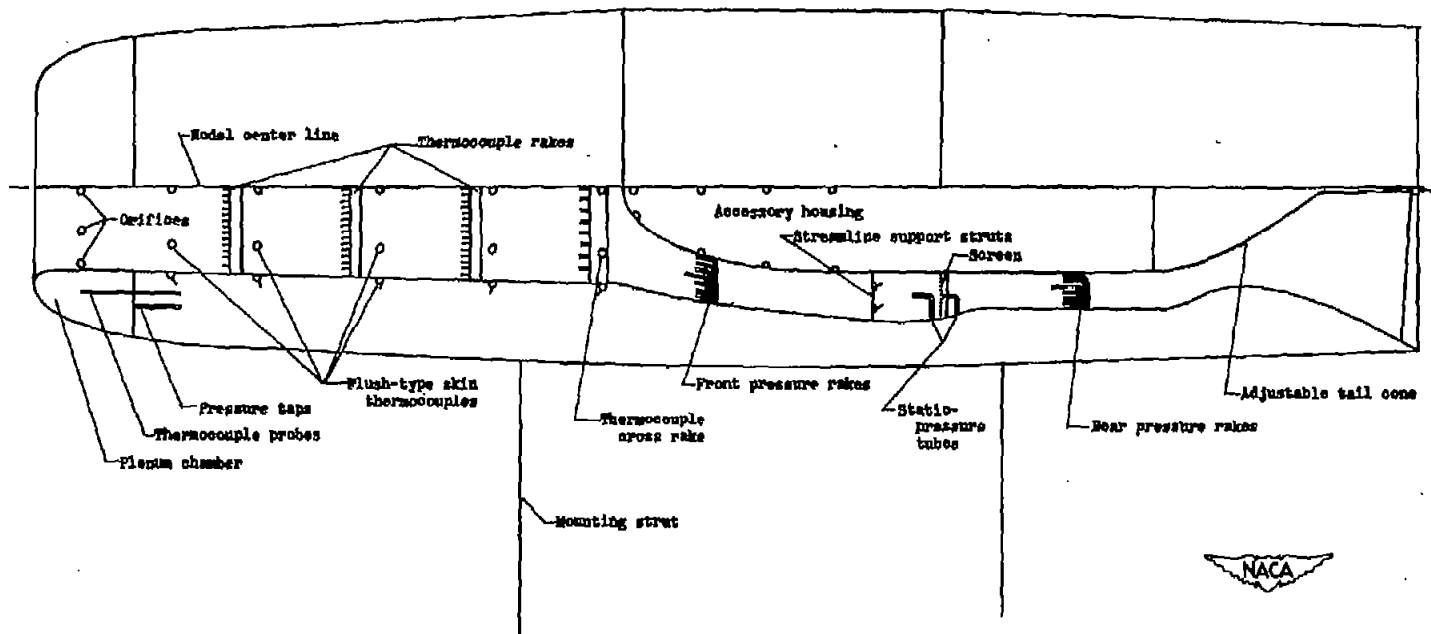
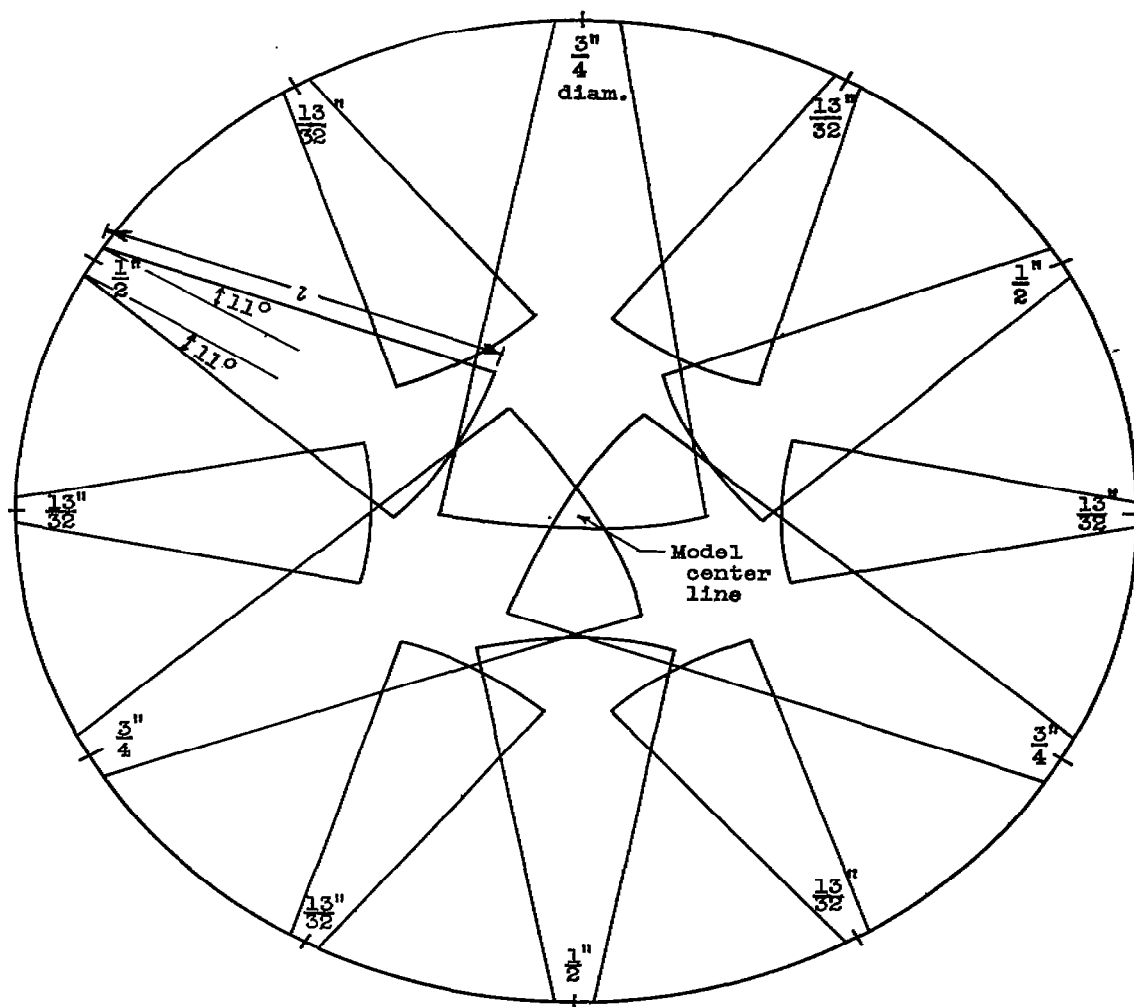


Figure 2. - Sketch of model showing instrumentation used in investigation.



NACA

Figure 3. - Sketch showing calculated jet outlines at accessory-housing tip using orifice configuration at inlet consisting of three  $3/4$ -inch, three  $1/2$ -inch, and six  $13/32$ -inch orifices.

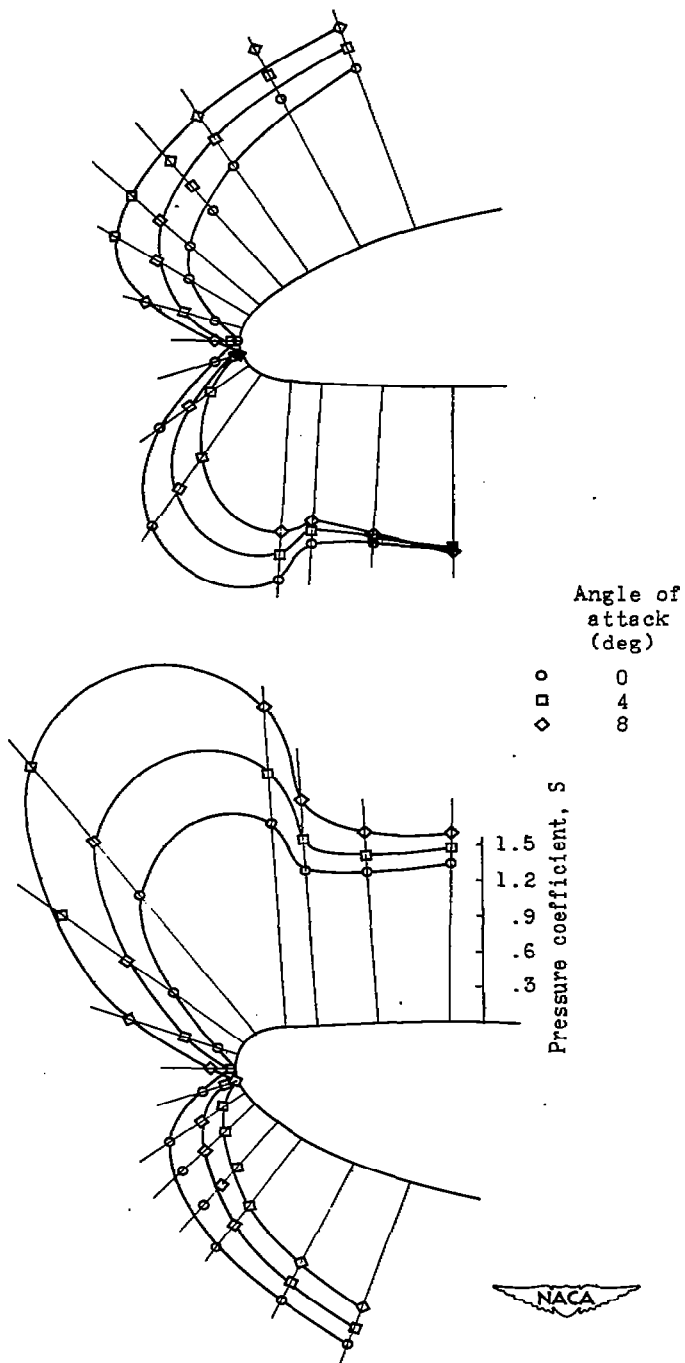


Figure 4. - Effect of angle of attack on lip-pressure distribution without bleedback.

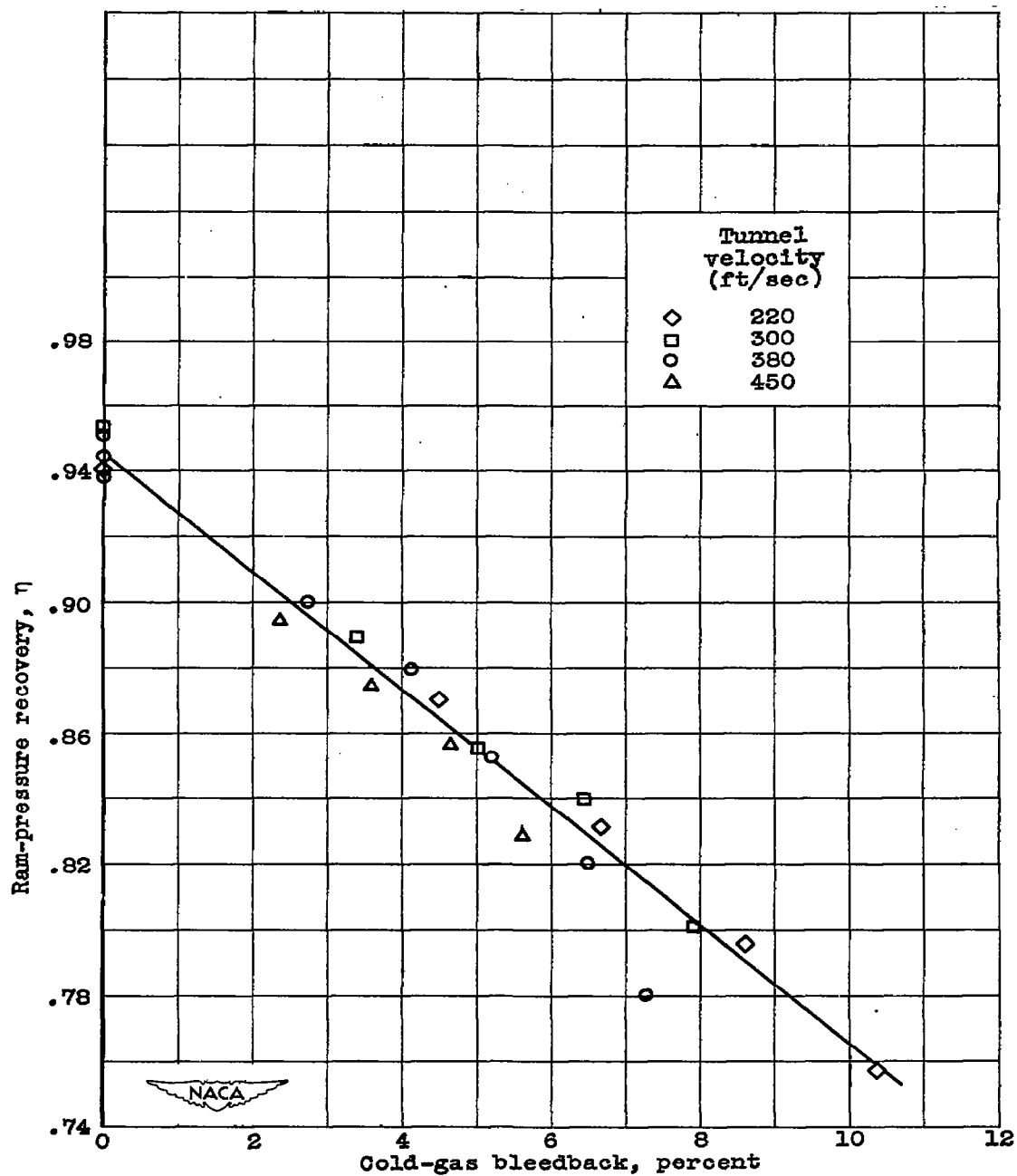


Figure 5. - Variation of ram-pressure recovery with cold-gas bleedback. Free-stream total temperature,  $0^{\circ}$  F; angle of attack,  $0^{\circ}$ .

1105

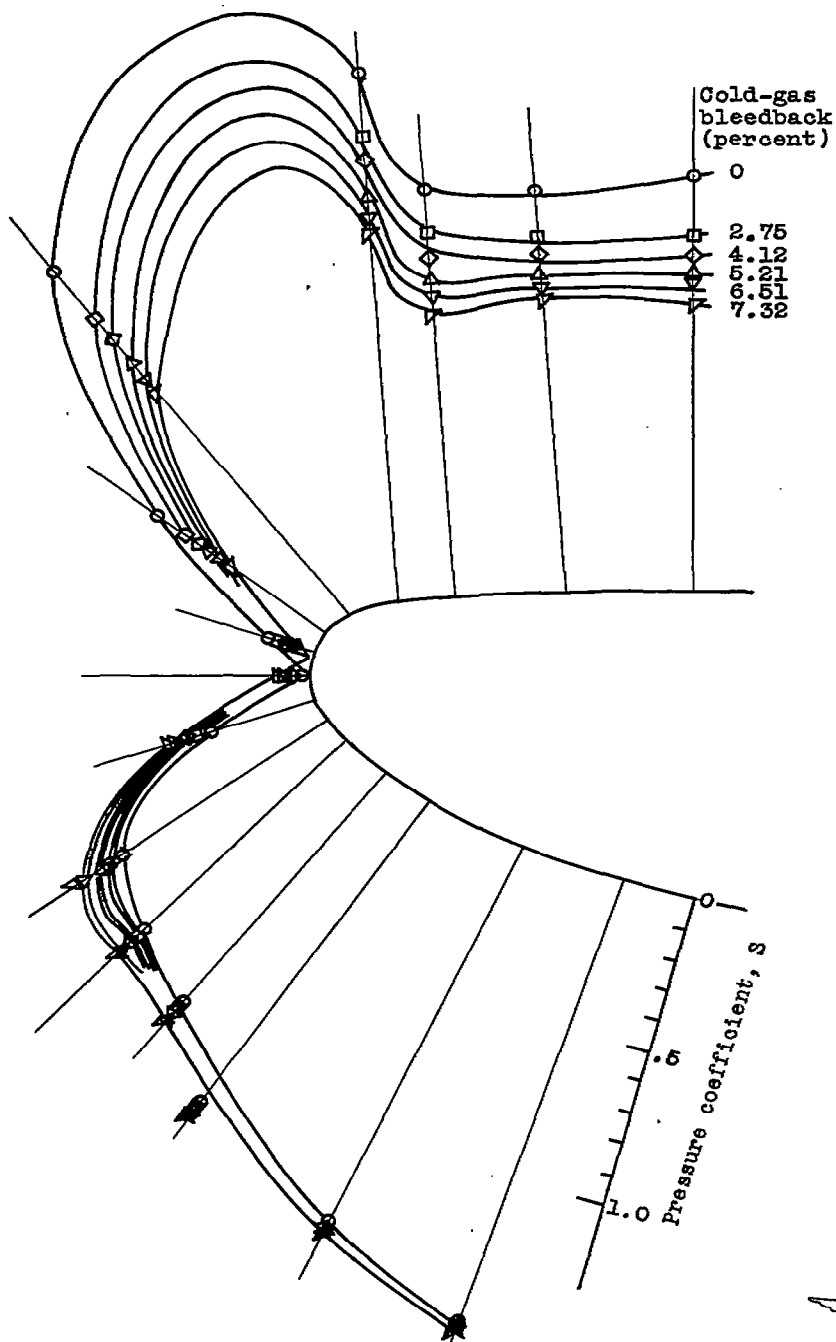


Figure 6. - Effect of cold-gas bleedback on lip-pressure distribution. Free-stream total temperature,  $0^{\circ}$  F; angle of attack,  $0^{\circ}$ .

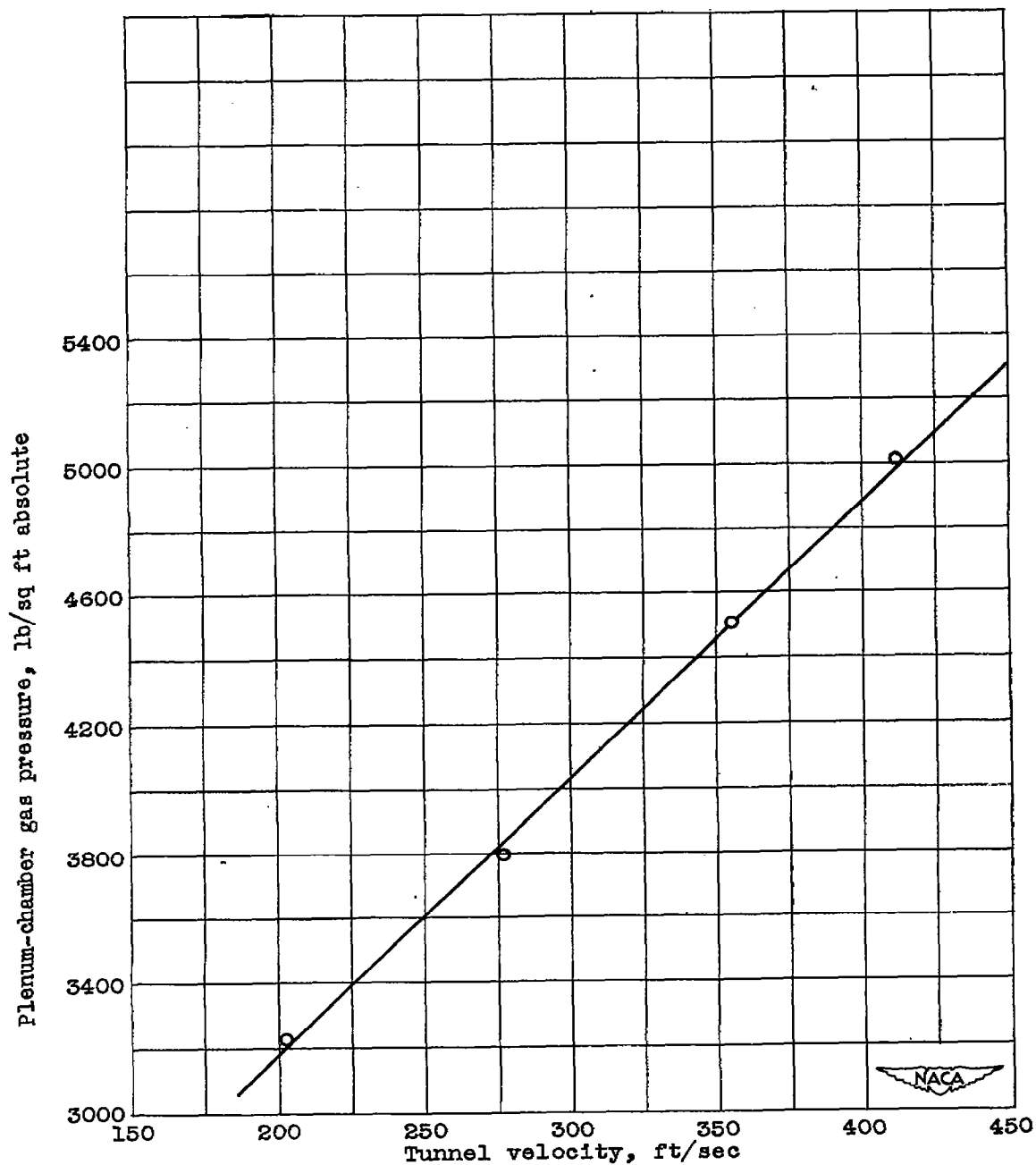
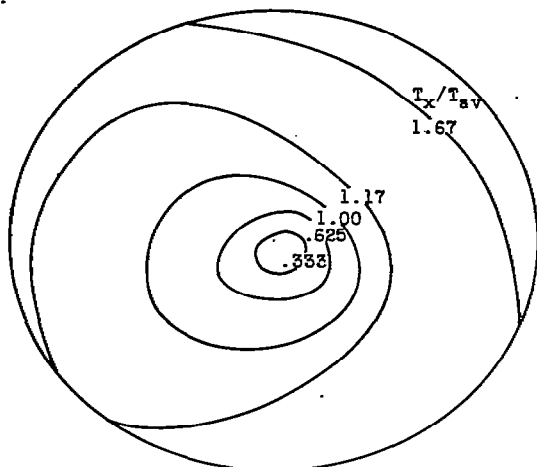
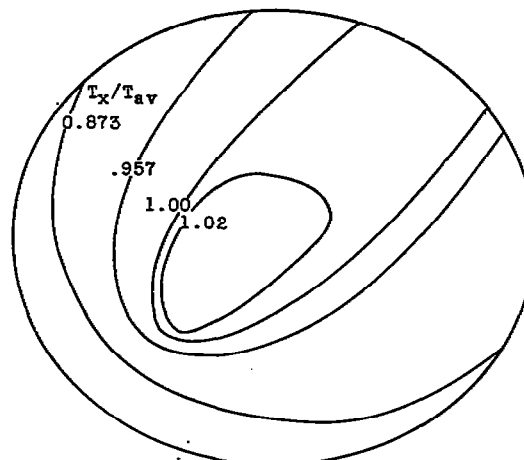


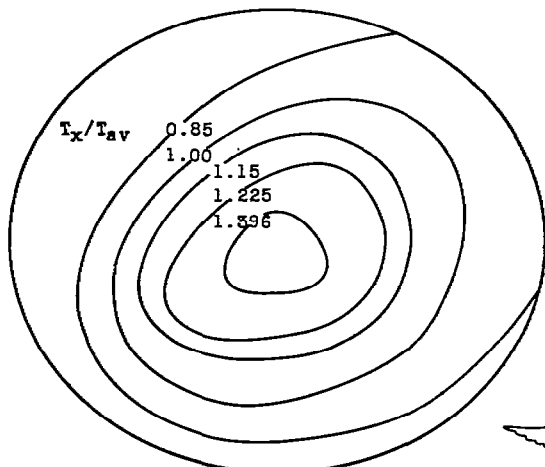
Figure 7. - Relation between plenum-chamber gas pressure and tunnel velocity corresponding to optimum temperature distribution in model. Plenum-chamber gas temperature, 1000° F.



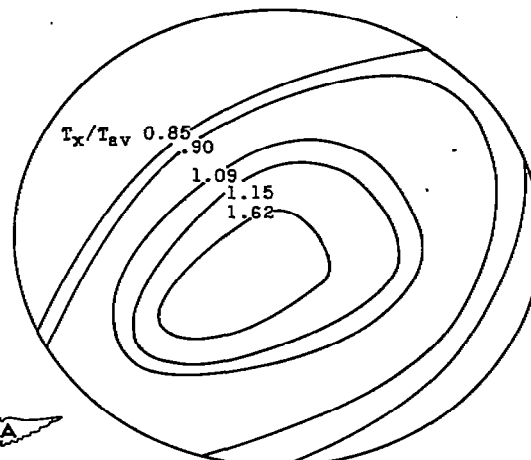
(a) Plenum-chamber gas pressure, 3010 pounds per square foot absolute; rise in model-air total temperature,  $33^{\circ}$  F; bleedback, 3.14 percent.



(b) Plenum-chamber gas pressure, 3950 pounds per square foot absolute; rise in model-air total temperature,  $46^{\circ}$  F; bleedback, 4.38 percent.



(c) Plenum-chamber gas pressure, 5100 pounds per square foot absolute; rise in model-air total temperature,  $64^{\circ}$  F; bleedback, 6.38 percent.



(d) Plenum-chamber gas pressure, 5840 pounds per square foot absolute; rise in model-air total temperature,  $74^{\circ}$  F; bleedback, 7.49 percent.



Figure 8. - Effect of plenum-chamber gas pressure on temperature ratio  $T_x/T_{av}$  at thermocouple cross rake. Tunnel velocity, 290 feet per second; plenum-chamber gas temperature,  $1000^{\circ}$  F; angle of attack,  $0^{\circ}$ .

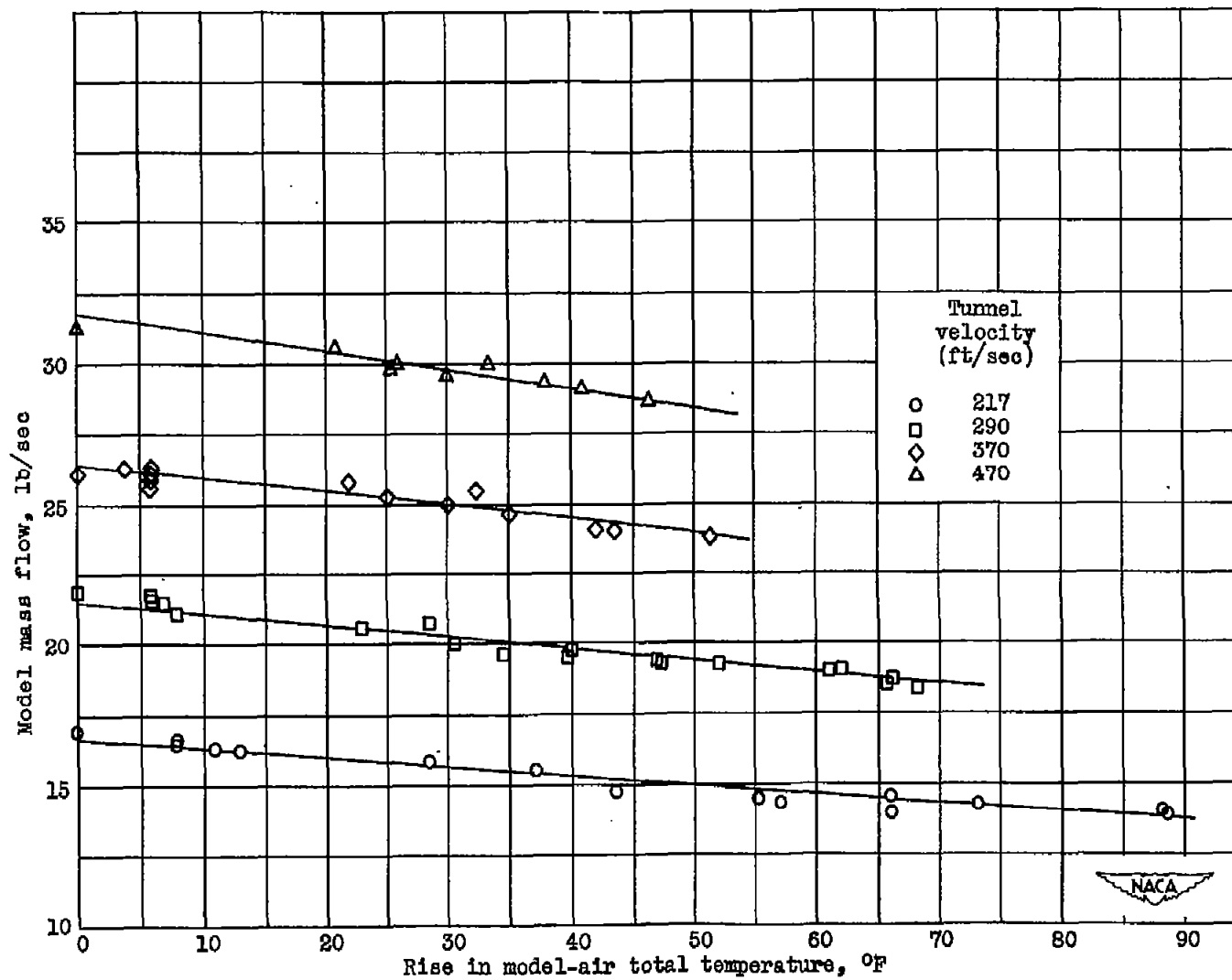


Figure 9. - Variation of mass air flow through model with rise in model-air total temperature for various tunnel velocities. Angle of attack,  $0^\circ$ ; free-stream total temperature,  $0^\circ$  F.

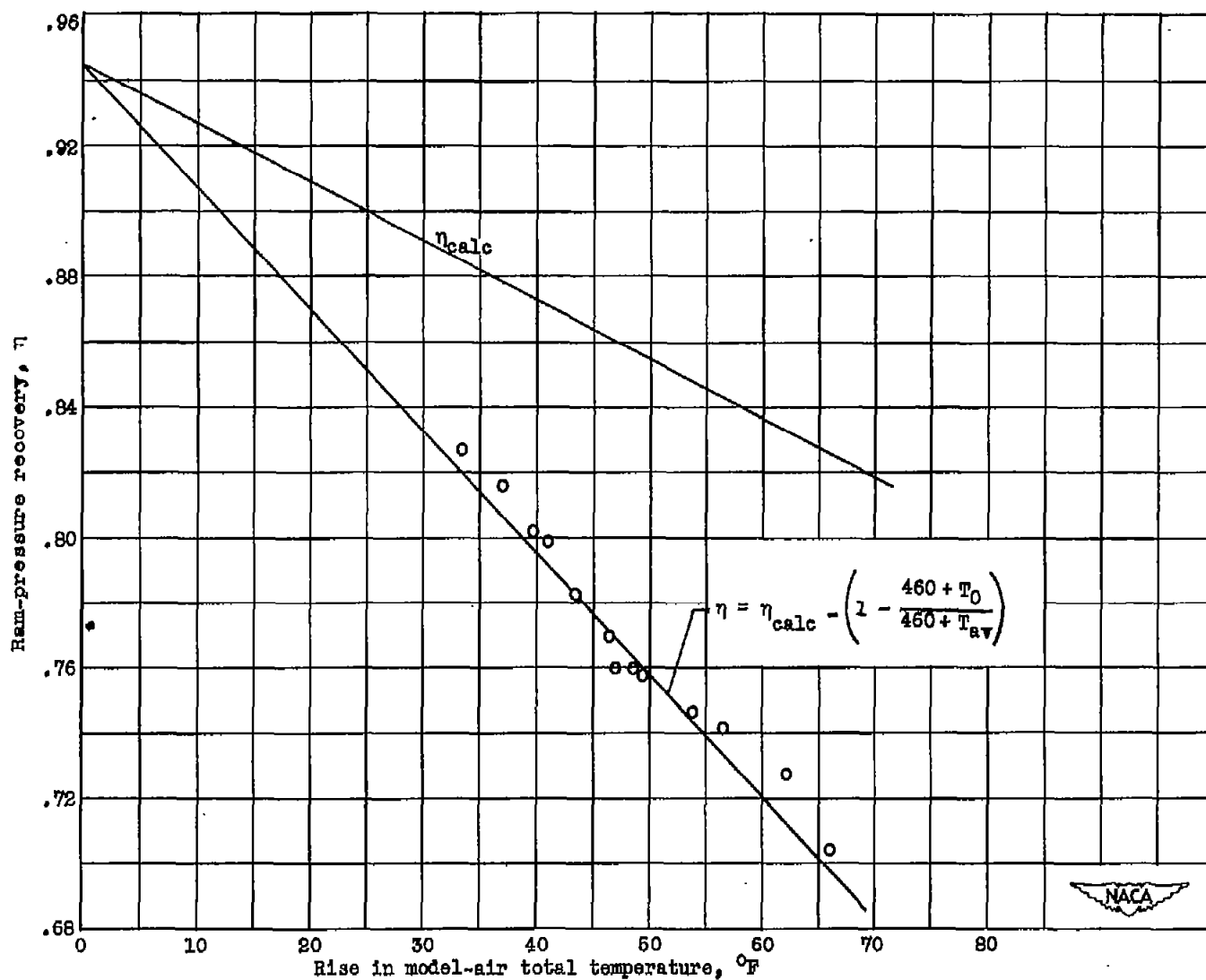


Figure 10. - Variation of ram-pressure recovery with rise in model-air total temperature for plenum-chamber gas temperature of  $1000^{\circ}\text{F}$ . Angle of attack,  $0^{\circ}$ ; free-stream total temperature,  $0^{\circ}\text{F}$ .

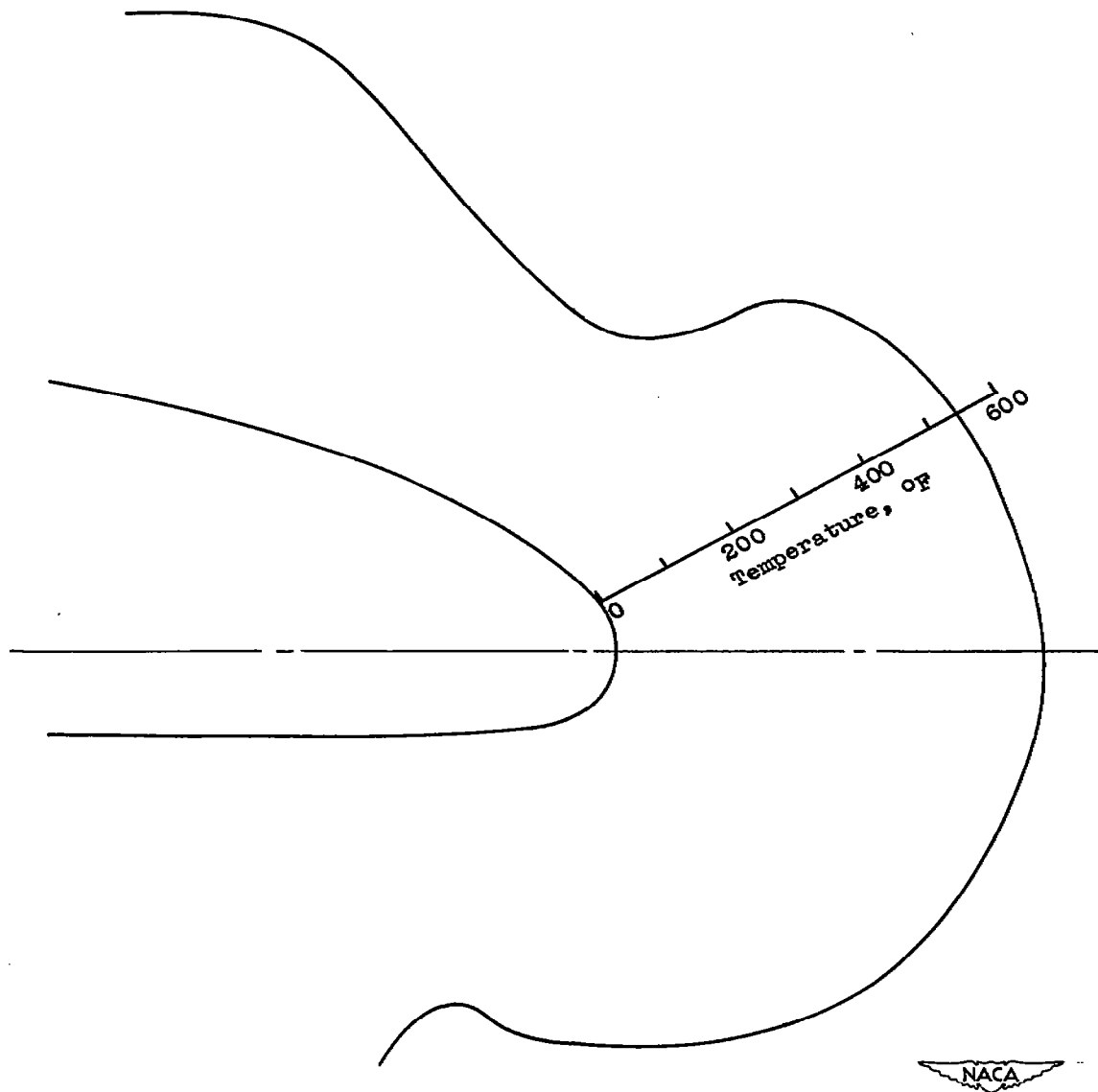


Figure 11. - Maximum inlet-lip temperature observed in investigation. Bleedback, 8.65 percent; plenum-chamber gas temperature,  $1000^{\circ}$  F; tunnel velocity, 218 feet per second.

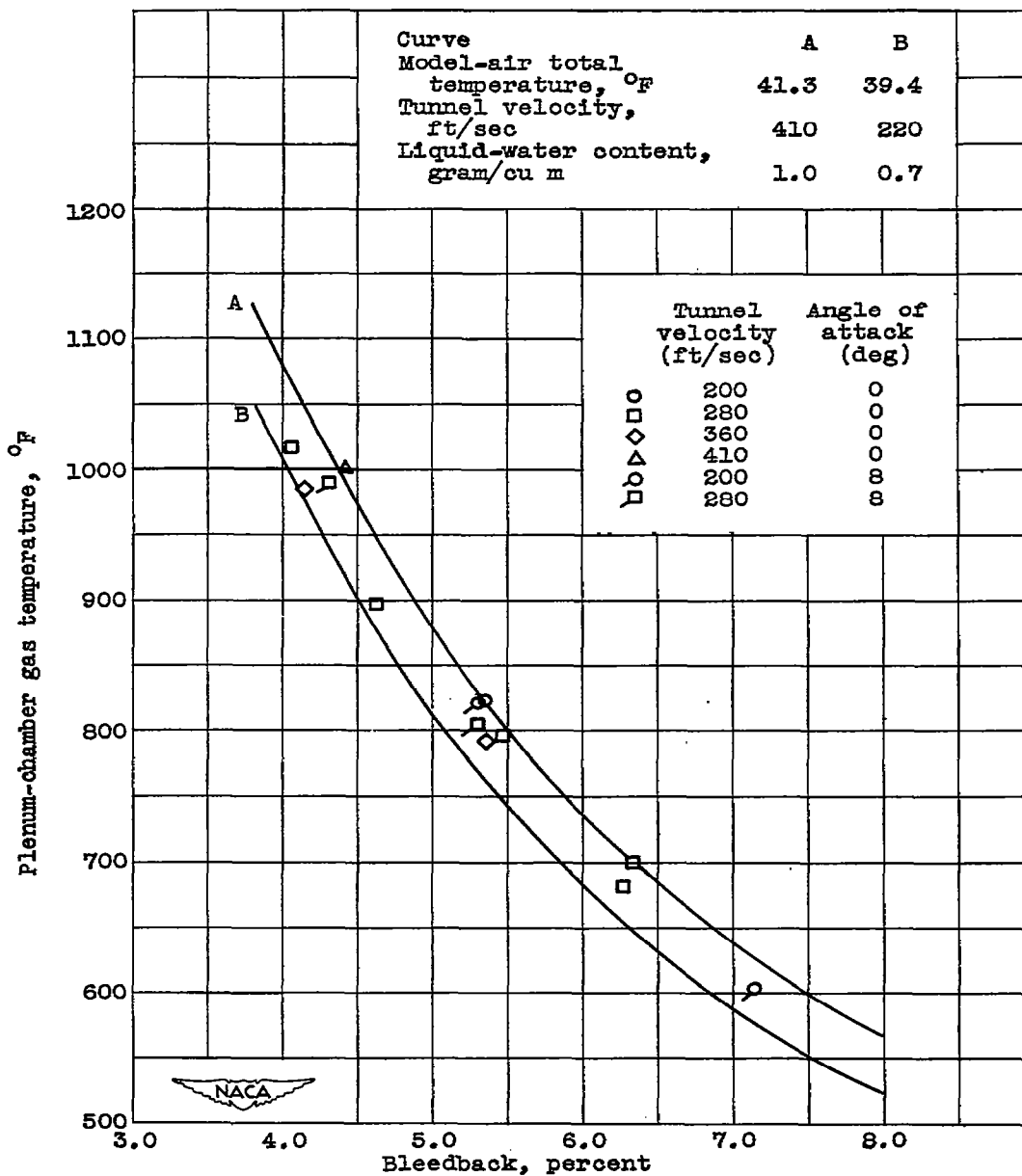


Figure 12. - Bleedback required for ice prevention as function of plenum-chamber gas temperature for free-stream total temperature of 0° F.

1105

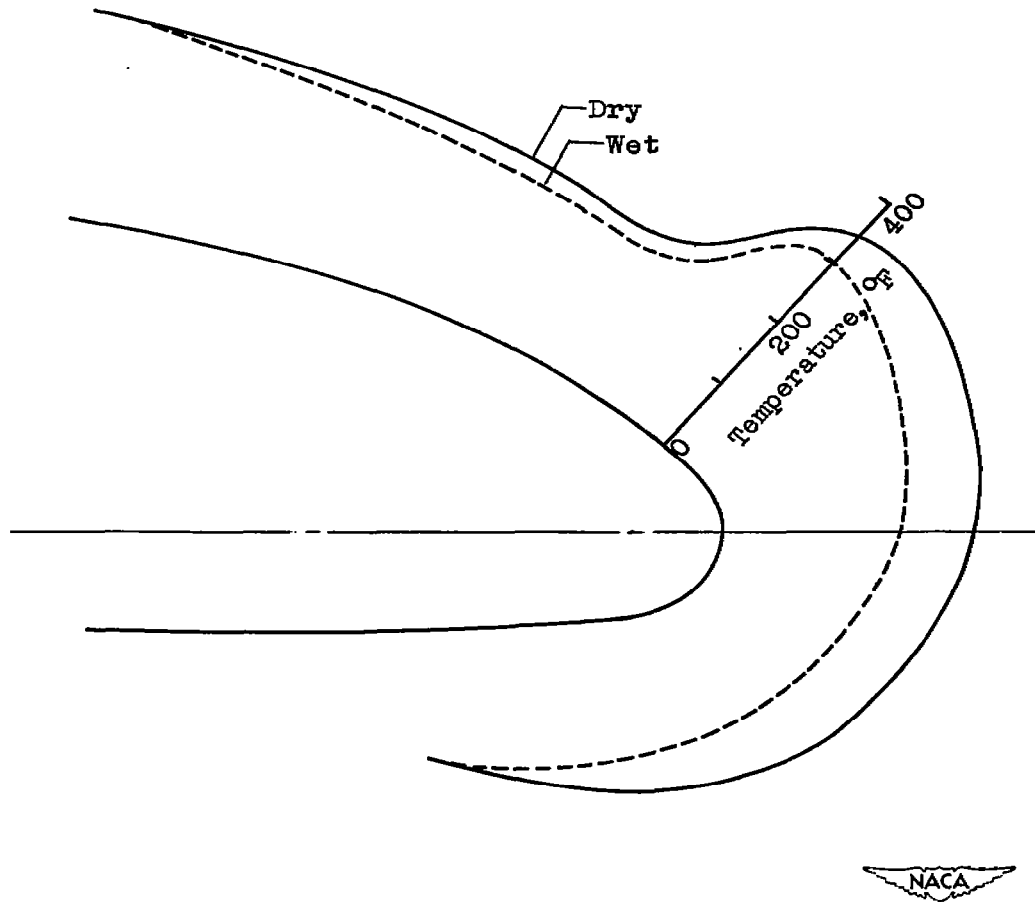


Figure 13. - Inlet-lip temperature distributions for dry air and icing conditions. Bleedback, 4.4 percent; plenum-chamber gas temperature, 1000° F; icing condition, liquid-water content of 0.5 gram per cubic meter at free-stream total temperature of 0° F.

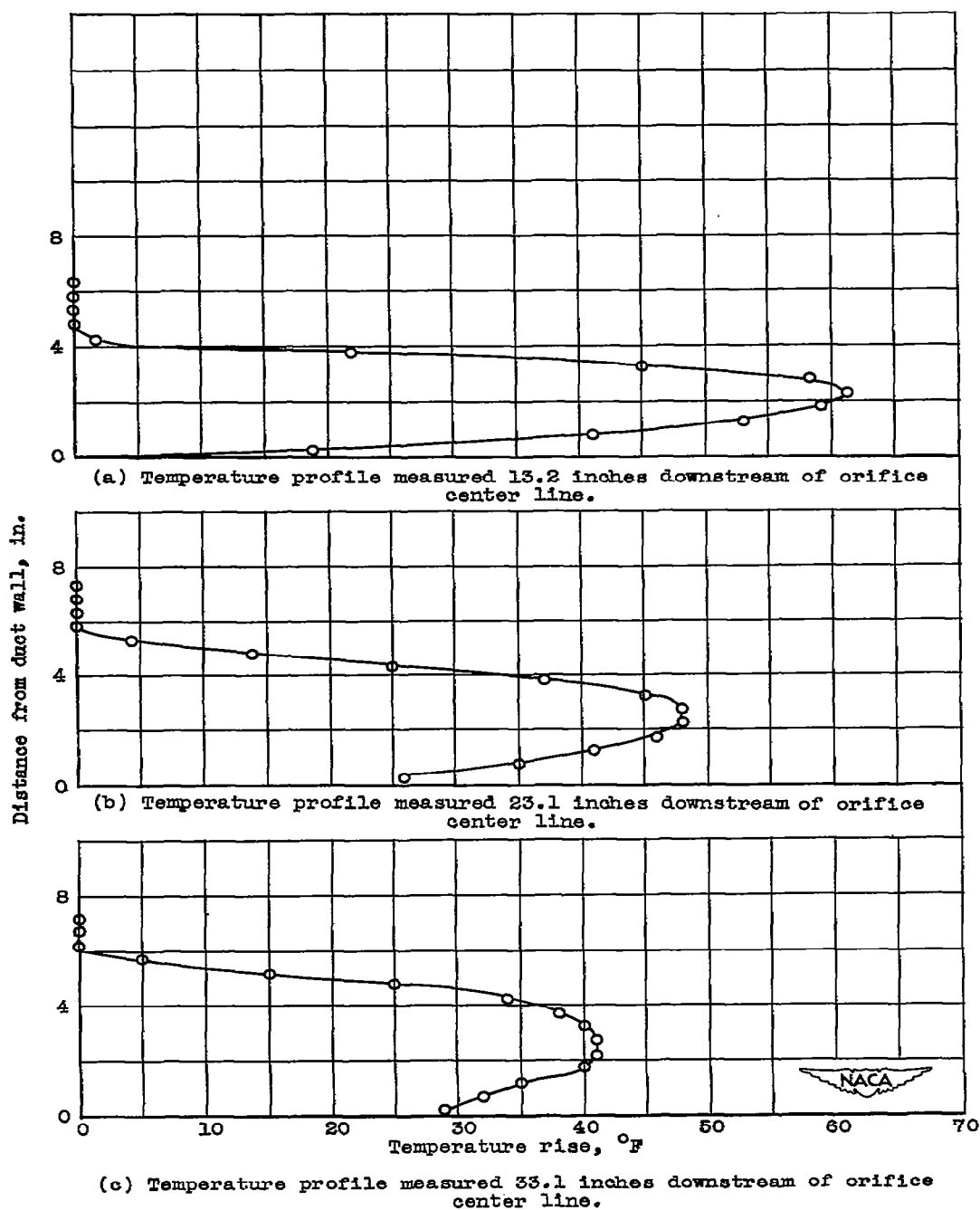


Figure 14. - Typical temperature profiles measured 13.2, 23.1, and 33.1 inches downstream of 3/4-inch-diameter orifice. Tunnel velocity, 374 feet per second; plenum-chamber gas temperature, 837° F; plenum-chamber gas pressure, 2900 pounds per square foot absolute.

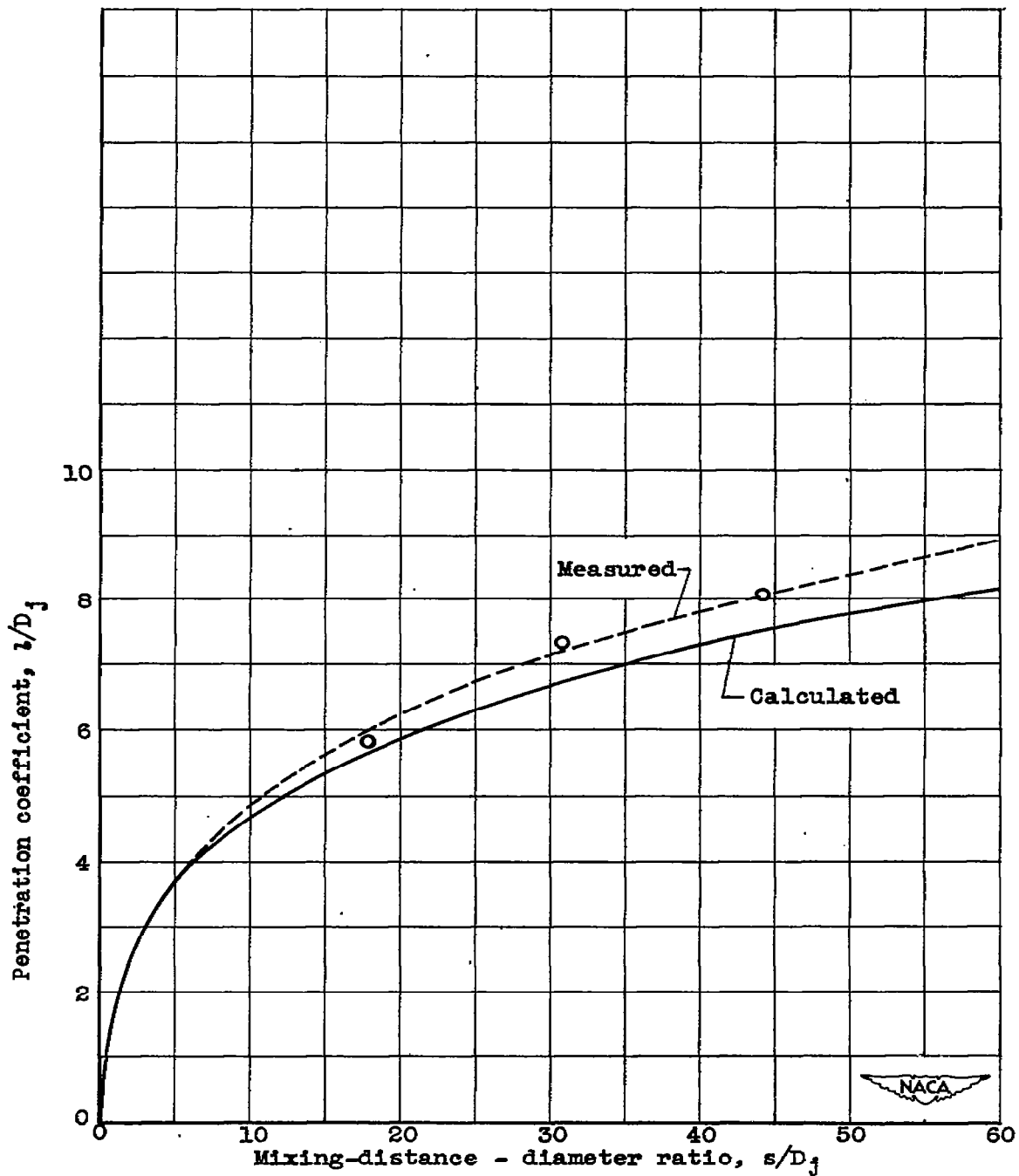


Figure 15. - Comparison of measured and calculated penetration coefficients as function of mixing-distance - diameter ratio.